Multielectron spectroscopy: Auger decays of the krypton 3*d* hole

J. Palaudoux,[1,2,*] P. Lablanquie,[1,2] L. Andric,[1,2,3] K. Ito,[4] E. Shigemasa,[5] J. H. D. Eland,[6] V. Jonauskas,[7] S. Kučas,[7] R. Karazija,[7] and F. Penent[1,2]

[1]*Laboratoire de Chimie Physique–Matière et Rayonnement, Université Pierre et Marie Curie, 11 rue Pierre et Marie Curie, F-75231 Paris Cedex 05, France*

[2]*CNRS, Laboratoire de Chimie Physique–Matière et Rayonnement (UMR 7614), 11 rue Pierre et Marie Curie, F-75231 Paris Cedex 05, France*

[3]*Université Paris-Est, 5 boulevard Descartes, F-77454 Marne-la Vallée Cedex 2, France*

[4]*Photon Factory, Institute of Materials Structure Science, Oho, Tsukuba 305-0801, Japan*

[5]*Ultraviolet Synchrotron Orbital Radiation Facility, Institute for Molecular Science, Okazaki 444-8585, Japan*

[6]*Department of Chemistry, Physical and Theoretical Chemistry Laboratory, Oxford University, South Parks Road, Oxford, OX1 3QZ, United Kingdom*

[7]*Institute of Theoretical Physics and Astronomy of Vilnius University, A Goštauto 12, Vilnius LT01108, Lithuania*

(Received 22 June 2010; published 19 October 2010)

The emission of one or two Auger electrons, following Kr 3*d* inner-shell ionization by synchrotron light, has been investigated both experimentally and theoretically. All electrons emitted in the process are detected in coincidence and analyzed in energy thanks to a magnetic-bottle electron time-of-flight spectrometer. In addition, noncoincident high-resolution electron spectra have been measured to characterize the cascade double-Auger paths more fully. Combination of the two experimental approaches and of our calculations allows a full determination of the decay pathways and branching ratios in the case of Kr 3*d* single- and double-Auger decays. The Kr^{3+} threshold is found at 74.197 ± 0.020 eV.

DOI: 10.1103/PhysRevA.82.043419 PACS number(s): 32.80.Hd, 32.70.Cs, 32.70.Fw, 32.80.Aa

I. INTRODUCTION

Auger electron spectroscopy is a powerful technique to investigate the decay of inner-shell hole states and provides specific information on the target atom and its chemical environment. Single-Auger emission is often described as a two-step process: in the first step an electron is ejected from an inner shell (by photon, electron, or ion impact) and, in the second step, this vacancy is filled by another electron falling from an upper shell while, to fulfill energy conservation, a third electron, the Auger electron, leaves the atom. This nonradiative process which competes with x-ray emission results from Coulomb interaction between electrons, and the energy of the emitted Auger electrons depends only on the energies of the intermediate core-hole state and of the different accessible final states specific to the element. The double-Auger process, where two Auger electrons can be ejected after inner-shell ionization, was observed for the first time by Carlson *et al.* in 1965 [1]. The ejection of two Auger electrons can be simultaneous or sequential. In the former case, the electrons share the available energy with a continuous distribution while, in the latter case, a cascade is observed that goes through a well-defined intermediate state and gives discrete energies.

Auger spectra can be very complex since they result from the superposition of Auger lines due to different initial vacancies and can involve cascade Auger decay; in molecules vibrational excitation in intermediate and final states makes the interpretation even more difficult [2]. However, the interpretation can be simplified by detecting the Auger electrons in coincidence with photoelectrons. Nowadays several electron-electron coincidence experiments have proved their ability to disentangle the complexity of Auger spectra; see, for instance, Refs. [3–14]. In these experiments, the photoelectron is measured in coincidence with one, two, or three Auger electrons, providing a complete and precise insight into the ionic states involved, often previously unknown, as well as into the mechanisms of the decay process.

The first Kr 3*d* Auger spectrum was reported by Mehlhorn in 1965 [15]. A higher resolution measurement by Werme *et al.* appeared in 1972 [16] and its interpretation was given by Mc Guire in 1975 [17]. Improvements in Auger electron spectroscopy techniques, such as higher resolution and the use of synchrotron radiation excitation, led then to better experimental observations mainly by the Finnish group in Oulu which also performed high-accuracy theoretical calculations [18–20]. More sophisticated calculations were published by Jonauskas *et al.* in 2008 [21]; the present theoretical investigations develop and extend this work.

Several experimental studies of the decay of the Kr $3d^{-1}$ states have used photoelectron-ion coincidence techniques with synchrotron radiation [22,23]; they pointed out that Kr^+ $3d^{-1}$states decay predominantly (about 70%) toward Kr^{2+} final ionic states but can also end up forming triply charged Kr^{3+} ions by double-Auger decay, with probabilities of 31% and 29% for $3d_{3/2}^{-1}$ and $3d_{5/2}^{-1}$, respectively [23]. The last class of experiments explores Kr 3*d* Auger decays by the use of coincidences between photoelectron and Auger electrons. Hikosaka *et al.* [4] used a threshold photoelectron detector and could disentangle Auger lines issued from the $3d_{3/2}$ and $3d_{5/2}$ subshells; they also reached a "subnatural linewidth regime" where the total energy resolution with which the Kr final states are observed is below the Kr 3*d* 88 ± 4 meV [24] natural linewidth. Viefhaus *et al.* [6] observed the double-Auger decays of Kr 3*d* holes with their angle resolved electron-electron time-of-flight (TOF) spectrometers.

*jerome.palaudoux@upmc.fr

By detecting in coincidence two electrons out of the three involved in the double-Auger process, they showed that cascade processes dominate over simultaneous ones. They also reported a precise energy level diagram of Kr^{3+} ion. Recently, Penent *et al.* [25] investigated both by theory and experiment how the double-photoionization channels are affected in the vicinity of the 3*d* thresholds, where postcollisional interaction (PCI) effects are huge.

In this paper, we present an extensive study combining experiment and theory, of both single- and double-Auger processes following the creation of the Kr^+ $3d^{-1}$ state. The experimental technique relies on a magnetic-bottle spectrometer implemented for use with synchrotron radiation [5]. The complete images of single- and double-Auger processes are obtained by the coincident detection of all (up to two here) subsequent Auger electrons with the photoelectrons. The method is characterized by its very high detection efficiency and good energy resolution as demonstrated in recent studies on the decay of Ar 2*p* [10], Xe 4*d* [5], and Xe 4*p* [11] holes. Preliminary results concerning our study of Kr 3*d* decays were already reported [12,26,27]. These results are completed here by high-resolution measurements obtained with a noncoincident electrostatic electron spectrometer and by theoretical calculations, in order to reach a better identification of all the processes.

II. EXPERIMENTAL PROCEDURE

Two different experimental setups have been used: a magnetic-bottle time-of-flight analyzer for its powerful coincidence detection and a high-resolution hemispherical analyzer for the spectroscopic characterization of the Kr^{2+} states involved in the cascade double-Auger decay.

The noncoincident high-resolution spectra were obtained on the BL6U undulator beamline at the Ultraviolet Synchrotron Orbital Radiation (UVSOR) storage ring in the Institute for Molecular Science in Okazaki, Japan. BL6U is equipped with a grazing incidence monochromator without an entrance slit containing a varied line-spacing plane grating. We used a high-performance hemispherical electron energy analyzer MBS-A1, developed by MB Scientific AB. It is equipped with a gas cell and a CCD camera and reaches a theoretical 1.3 meV [full width half maximum (FWHM)] resolution when operated at a pass energy of 2 eV and a slit opening of 0.2 mm. The energy scale was autocalibrated on the strongest Kr 3*d* double-Auger cascade peak at 0.727 eV, a value that we obtained with the magnetic-bottle analyzer.

The main part of the experimental results was obtained with a magnetic-bottle time-of-flight electron coincidence spectrometer of the type developed by Eland *et al.* [28]. This setup was previously described in detail in Refs. [5,10]. The experiment was performed at BESSY II on beam line UE 56/2 PGM1, during the single bunch operation mode of the synchrotron which provides light pulses every 800.5 ns. Briefly, a small ($\Phi = 24$ mm, $L = 40$ mm) conical-shaped, strong permanent magnet (0.7 T) placed close ($\sim$1 mm) to the interaction region (crossing of the photon beam with the target gas effusing from a 500 μm inner diameter needle) creates a highly inhomogeneous magnetic field that acts as a magnetic mirror, repelling most (>90%) of the electrons into the homogeneous magnetic field (1 mT), created by a long solenoid (2 m). After parallelization of their trajectories in the "bottleneck" in a few centimeters, electrons are guided by the solenoid field to a detector (a set of three microchannel plates of 40 mm active diameter followed by a phosphor screen anode with an indium tin oxide conductive coating). The fast electron signal collected on the anode is sent to a multihit time-to-digital converter (TDC) that measures the time of arrival of the electrons with respect to the synchrotron ring clock with a 250 ps time resolution. A mechanical chopper similar to the one described by Hikosaka *et al.* [29] and Ito *et al.* [30] was used to reduce the light pulse period to $\sim$12 μs to allow absolute time-of-flight measurement of the electrons when the electron time of flight is longer than the single bunch period of 800.5 ns. Time-to-energy calibration was performed for electron kinetic energies from 0 to 200 eV by measuring helium photoelectron TOF at known photon energies (and cross-checked with known krypton Auger electron energies). In order to obtain time-to-energy conversion, a simple formula of the type $t = t_0 + \frac{D}{\sqrt{E+E_0}}$ is used, later improved by adding correction terms to take into account the effect of electric potential variations along the electron trajectories as described previously in [10]. The good energy resolution, due to the 2-m-long flight path, is one of the advantages of this experiment; it can reach $\Delta E = 10$ meV for electrons of less than 1-eV kinetic energy, while $\Delta E/E = 1.6\%$ for higher energies. The detection efficiency that combines the collection solid angle of the magnetic bottle and the detection of the electrons by microchannel plates is determined to be 54% $\pm$ 3% by the ratio of the Auger spectrum measured in coincidence with the photoelectron to the total Auger spectrum (where Auger electrons are observed with or without coincidence with the photoelectron).

The krypton electronic configuration is $[Ar]3d^{10}4s^24p^6$. The energy thresholds to remove a 3*d* electron are given by King *et al.* [31] at 93.788 eV (Kr^+ $3d_{5/2}^{-1}$) and 95.038 eV (Kr^+ $3d_{3/2}^{-1}$). The krypton double-ionization threshold (Kr^{2+} $4p^{-2}\,{}^3P_2$) is given by NIST at 38.358 eV [32]. The triple ionization threshold given in the literature [32,33]) at 75.308 eV is known to be overestimated by around 1 eV, as was demonstrated by several authors [6,26,34]; we will come back to this point later in the paper. Since double- and triple-ionization thresholds lie below the Kr^+ $3d^{-1}$ threshold, the decay of 3*d* holes to Kr^{2+} and Kr^{3+} states by single- and double-Auger decay is possible.

We present in Fig. 1 the raw absolute time-of-flight spectra observed at an incident photon energy $h\nu = 127$ eV. At this photon energy, the kinetic energy of photoelectrons is about 35 eV. The single-Auger electrons have a maximum energy of 55 eV, and double-Auger electrons have about a maximum of 20 eV to share. The energy resolution of our apparatus is around 0.8 eV at 50 eV, so we can easily resolve $3d_{5/2}$ and $3d_{3/2}$ photoelectrons, which allows us to select the initial core-hole state when studying the Auger process.

Figure 1 gives a first insight into all observed processes which will be detailed in Sec. 4. Figure 1(a) presents the histogram of all detected electrons. The $3d_{3/2,5/2}^{-1}$ photoelectron peaks which are separated by 1.25 eV are easily identified (at 588 and 600 ns). We can also attribute the peaks at 310 and 332 ns to valence ionization (in 4*p* and 4*s* shells,

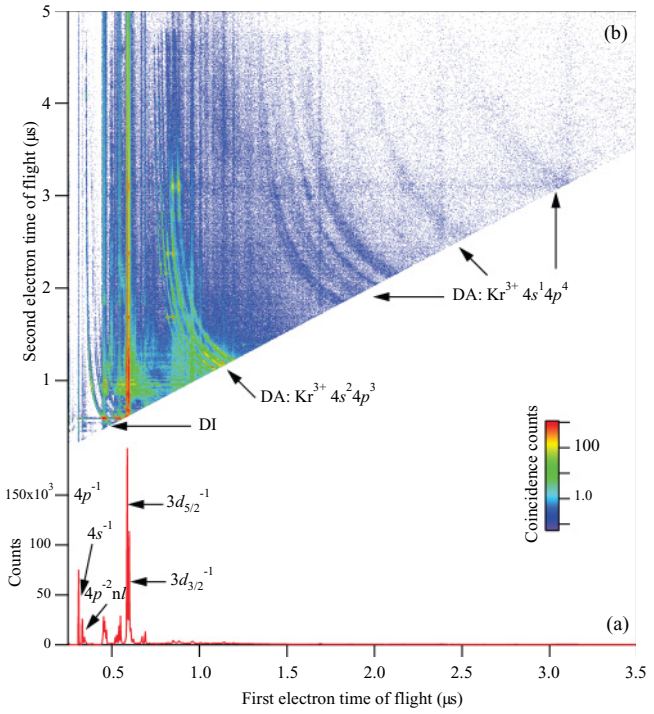

FIG. 1. (Color online) (a) Histogram of the time of flight of all detected electrons. (b) The two-dimensional picture presents all coincidences recorded between two electrons. Counts (i.e., z axis in 2D picture) are given on a logarithmic scale. The photon energy was 127 eV, accumulation time was 3 h, and the count rate was maintained constant at 2200 Hz.

respectively). They are followed by $4p$ satellite states (one $4p$ electron removed with another $4p$ excited, i.e., $4p^{-2}$ nl configurations). In the two-dimensional (2D) map [Fig. 1(b)], the coincidences between a $4p$ or a $4s$ photoelectron and another electron are accidental coincidences. The end of this $4p^{-2}$ nl series ($n \to \infty$) corresponds to the valence double-photoionization (DI) process, which cannot be isolated in the one-dimensional spectrum. But the DI paths are clearly seen in the 2D map [Fig. 1(b)] which records all two electron coincidences, as weak "hyperbolic-like" curves. On Fig. 1(b), we also identify for $T_1 = 588$ and 600 ns the stronger process which corresponds to coincidences between $3d$ photoelectrons and Auger electrons (vertical features); note the associated horizontal lines at $T_2 = 588$ and 600 ns which corresponds to events where the Auger electron is faster than the photoelectron. Different families of hyperbolic-like curves are also clearly visible on the 2D spectra. The strongest one, around $T_1 \approx 1$ μs, corresponds to double-Auger (DA) decay to the triply charged Kr^{3+} $4p^{-3}$ final state. At this photon energy, it overlaps with vertical features in the 2D map, which correspond to the $3d^{-1}4p^{-1}nl$ photoelectron satellites detected in coincidence with the associated Auger electrons. We may note in a similar way the associated horizontal lines around 1 μs when the Auger electron is faster than the photoelectron satellites. Core-valence $3d^{-1}4p^{-1}$ or $3d^{-1}4s^{-1}$ double ionization begins where the $3d$ satellite states end up and correspond to some of the "hyperbolas" at $T_1 \approx 1.5$–2 μs; they partly overlap with double-Auger decay of $3d$ holes to Kr^{3+} $4p^{-2}4s^{-1}$ whose hyperbolas extend up to $T_1 \approx 2$–3 μs. The hyperbola-like curves associated with the coincidences between two Auger electrons in the double-Auger (direct or in cascade) decay do not depend on the photon energy while core-valence double-photoionization curves move with the photon energy. The double-Auger decay paths can also be easily filtered from the overlapping phenomena by considering triple coincidence events in which one detects the $3d_{3/2,5/2}$ photoelectron in coincidence with two Auger electrons. This will be discussed in detail in Sec. 4.2 while core-valence double ionization and its Auger decay have been examined in detail in Gamblin's Ph.D thesis [35] and will be developed in a forthcoming paper. In the 2D map of Fig. 1(b), faint horizontal and vertical lines linked to intense coincidence spots, like the ones at $T = 1.7$ or 3.1 μs are due to accidental coincidences. The process is of almost negligible intensity but its visibility is enhanced by the logarithmic scale. This 2D map also clearly demonstrates a cutoff at $T_2 \approx 4.8$ μs of the coincidence counts which corresponds to the time of flight of zero kinetic energy electrons; these arrive in a finite time because of the repelling potential of about -0.5 eV applied to the magnet. This potential value is a good compromise to retain good energy resolution for slow electrons while avoiding a too long time of flight during which random electrons could arrive. Coincidences for $T_2 > 4.8$ μs are false coincidences only, and can be statistical (noise) but can also result from secondary processes (electron or ion collisions on target gas or on surfaces, . . .). These false coincidences have not been subtracted from the 2D map since the procedure is tedious, but the count rates are kept to values for which such random coincidences are low enough to keep the true coincidence signal dominant. Moreover, by selecting three electron events, as in double-Auger decay, false coincidences are efficiently reduced in comparison with the 2D map.

III. THEORETICAL MODEL

The calculations of Auger decays of the krypton $3d_j$ vacancy states have been performed in the relativistic configuration interaction approximation using the flexible atomic code [36]. The set of configurations, mixing more strongly with the considered configuration, has been selected using the configuration interaction strength [37,38]. This measure of mixing between the configurations K and K' is determined as follows:

$$T(K,K') = \frac{\sum_{\gamma\gamma'} \langle K\gamma|H|K'\gamma'\rangle^2}{\bar{E}(K,K')^2}, \tag{1}$$

where the quantity in the numerator is the interconfiguration matrix element of the Hamiltonian H and $\bar{E}(K,K')$ is the energy distance between the interacting levels of configurations K and K':

$$\bar{E}(K,K') = \frac{\sum_{\gamma\gamma'} [\langle K\gamma|H|K\gamma\rangle - \langle K'\gamma'|H|K'\gamma'\rangle]\langle K\gamma|H|K'\gamma'\rangle^2}{\sum_{\gamma\gamma'} \langle K\gamma|H|K'\gamma'\rangle^2}. \tag{2}$$

The summation in (1) and (2) is performed over all states γ and γ' of both configurations.

Configuration interaction strength has been calculated between the considered configuration and several hundreds of configurations differing from it by states of two or one electrons. The strong interaction of some admixed configurations has been taken also into account. A set of configurations has been selected according to the largest values of $T(K,K')$. The following numbers of nl configurations in sets have been used: 29 for Kr^+, 140 for Kr^{2+}, and 80 for Kr^{3+}. They include discrete configurations with and without a $3d$ vacancy and various excitations from $4s$ and $4p$ shells up to $n = 11$ Rydberg states. All nlj configurations corresponding to various distributions of the electrons in the subshells of open shells have been included in the set.

The relative numbers of Auger electrons emitted in the transitions between the separate levels have been calculated in terms of the products of populations of initial levels and Auger transition rates. The expression for the population of levels follows from the condition that the number of deexciting atoms has not changed during the Auger cascade:

$$N(K\gamma) = \frac{\sum_{K'\gamma'} N(K'\gamma')A(K'\gamma' - K\gamma)}{\Gamma(K'\gamma')}, \qquad (3)$$

Here, $A(K'\gamma' - K\gamma)$ is the Auger transition rate and $\Gamma(K'\gamma')$ is the total natural width of the level or its total deexcitation rate.

The low-energy part of the Auger spectrum contains a large number of lines with small spacing between them, thus the theoretical values of the line intensities have been convoluted taking into account the natural and instrumental width as Voigt profiles using the method given by Zaghloul [39]. The fluorescence yield for the considered Kr^{2+} configurations differs considerably for various levels, thus the radiative natural width must be also taken into account, especially for the low part of the Auger spectrum, where the instrumental resolution can be smaller than the natural width.

We restrict our theoretical study of the double-Auger decay to the cascade double-Auger transitions involving a discrete intermediate state of doubly ionized krypton. These calculations are compared with the experimental spectra.

IV. EXPERIMENTAL RESULTS

A. Complete Auger spectra after Kr^+ $3d^{-1}$ decay

The Kr $3d$ Auger spectra were first recorded by Mehlhorn [15]. Noncoincident spectra at good resolution were then published by Werme *et al.* [16] and later by Aksela *et al.* [18] and Jauhiainen *et al.* [19] in the energy region 20–60 eV. Because of the 1.25 eV spin-orbit splitting of the Kr $3d_{5/2,3/2}$ subshells, the reported Auger spectra consist of Auger lines associated with both core vacancies. The observed spectral features are complicated not only because of the possible overlap of Auger lines associated with these two initial core-hole states but also because of the contribution of Auger lines associated with the decay of Kr^+ $3d^{-1}$ satellite states. The calculations of Mc Guire [17] and Jauhiainen *et al.* [19] are not in perfect agreement with the observed spectra concerning the positions and the intensities of the peaks, because the many-body and relativistic effects are difficult to tackle, making the precise identification of the peaks more complex.

Coincident experiments are extremely helpful in such cases thanks to the possibility of selecting the initial core-hole state of the Auger transition and consequently giving reliable identification of the observed transitions. The first coincident Auger spectra in krypton were reported by Hikosaka *et al.* [4] in the 30–59 eV energy region. Viefhaus *et al.* [6] then published coincident spectra including the low-energy region. Both experiments used synchrotron radiation excitation. Our magnetic-bottle spectrometer offers big advantages. Because of the very high collection efficiency over the $\sim 4\pi$ solid angle from 0 to 200 eV with a constant transmission, it is possible to detect in coincidence more than two electrons with a good resolution and to obtain directly the branching ratio without any correction for transmission. For double-Auger decay it is important to detect all three electrons in coincidence to remove possible ambiguities if only two are detected. The high efficiency also allows very high count rates in coincidence, giving excellent statistical accuracy in reasonable acquisition time (typically ~3 h). Our complete Auger electron spectra filtered by selection of the photoelectron $3d_{5/2,3/2}$ times of flight are presented in Fig. 2 after time-to-energy conversion. To obtain these spectra we used two different photon energies (124 and 130 eV) to compensate for the overlap (at those photon energies) of Auger electrons and

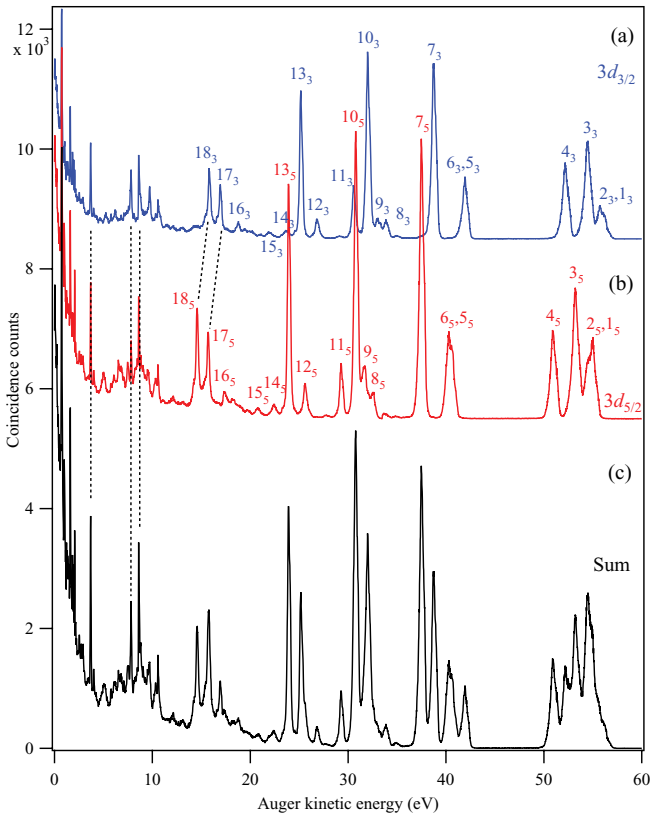

FIG. 2. (Color online) Complete Auger spectra in krypton (deduced from two measurements at 124 and 130 eV photon energy; see text for details). (a) (blue curve) Shows all Auger electrons detected in coincidence with a $3d_{3/2}$ photoelectron. (b) (red curve) Presents in a similar way the $3d_{5/2}$ Auger spectrum. (c) (black curve) Gives the sum of the spectra in (a) and (b).

TABLE I. Experimental and calculated Kr Auger spectra after $3d_{3/2}^{-1}$ and $3d_{5/2}^{-1}$ decays. The present table includes all single-Auger paths but lists only the first electron of cascade double-Auger processes. In other words it represents the Kr^{2+} states populated by the $3d$ decays. Auger lines are named with numbers as in Figs. 2 and 10, and also by capital letters, following the assignment of double-Auger spectra. Experimental values are from Fig. 2, E represents Auger kinetic energies, and I the branching ratios (in %). At this photon energy we observe a 1.45 ratio for the $3d_{5/2}/3d_{3/2}$ populations.

Line Designation		$3d_{3/2}^{-1}$ Experimental E (eV)	I	$3d_{3/2}^{-1}$ Calculated E (eV)	I	$3d_{5/2}^{-1}$ Experimental E (eV)	I	$3d_{5/2}^{-1}$ Calculated E (eV)	I	Leading Configuration of final Kr^{2+} state
1		56.3 ± 0.1	3.8	57.45	1.20	55.3	6.9	56.49	1.52	$4p^4\ ^3P_2$
2		56.0				54.9				$4p^4\ ^3P_{1,0}$
3		54.7	9.7	55.87	8.64	53.5	8.5	54.61	8.08	$4p^4\ ^1D$
4		52.5	6.8	53.67	3.82	51.3	5.4	52.39	3.00	$4p^4\ ^1S$
5		42.5	4.9	44.06	8.97	41.2	6.4	42.47	8.91	$4s4p^5\ ^3P_2$
6						40.8				$4s4p^5\ ^3P_{1,0}$
7		39.3	12.5	40.60	21.39	38.0	13.2	39.33	20.5	$4p^3 4d\ ^5D$
8		34.1	1.4	35.16	3.51	32.7	1.2	33.86	4.09	$4p^3 5s\ ^1P$
9		33.4	1.3	34.52	3.20	31.9	3.0	33.04	4.84	$4p^3 4d\ ^3D_{3,2,1}$
10		32.3	11.3	33.10	25.20	31.1	11.1	31.83	25.2	$4p^3 4d\ ^3P_{2,1}$
11		30.8	3.1	31.91	12.67	29.6	2.2	30.64	12.0	$4p^3 4d$
12		26.9	1.4	27.65	3.95	25.6	1.7	26.38	4.34	$4p^3 5d$
13		25.2	7.0	26.82	16.37	24.1	7.9	25.55	17.3	$4p^6\ ^1S$
14		23.9	0.9	25.21	0.82	22.6	0.9	23.97	0.60	$4p^3\ 5d^1$
				24.36	0.72			23.08	0.77	$4p^3\ 6d^1$
15		21.9	0.7	22.61	0.38	20.8	0.8	21.41	0.37	$4p^3\ nl$
16	$1F$	18.77	2.7	20.05	0.43	17.52	1.6	18.65	0.71	$4p^3\ nd$
17	$1B$	17.05	8.0	17.8	7.67	15.9	8.1	16.53	8.05	$4s4p^4 5s$
18	$1A$	16.0	12.0	16.56	4.79	14.8	11.5	15.26	5.19	$4p^2 4d^2$
21	$1C$	9.82	6.0	9.95	8.57	8.57	–	8.70	8.01	$4s^2 4p^2\ 5s^2$
22	$1D$	8.79	3.3	8.90	2.96	7.54	3.7	7.63	3.62	$4p^2 4d 5d$
23	$1E$	7.83	3.2	7.76	3.00	6.58	2.5	6.48	2.43	$4s4p^4 6d$
				7.25	2.17			5.97	2.24	$4p^2 4d^2$
24		6.26				5.05				

$3d$ photoelectrons around 30–35 eV. It was not possible to use higher photon energy because then we would not totally resolve the spin-orbit splitting $3d_{5/2}/3d_{3/2}$. All spectra were normalized on the area of nonaffected Auger lines. Figure 2(a) shows the Auger electrons detected in coincidence with $3d_{3/2}$ photoelectrons and Fig. 2(b) shows the Auger electrons created after $3d_{5/2}$ inner-shell ionization. The two spectra are very similar since they seem only shifted by 1.25 eV due to the fine structure $3d_{5/2}/3d_{3/2}$ [31]. Figure 2(c) represents the normal Auger spectrum in coincidence with either $3d$ photoelectrons obtained without discrimination of the two subshells. This spectrum can be directly compared with noncoincident spectra [16,18,19]. Thanks to the coincidence technique, one separates immediately and without ambiguity peaks resulting from $3d_{3/2}$ or $3d_{5/2}$ subshell ionization. Values of the Auger kinetic energies are reported in Table I. Similar tables have previously been published, sometimes with better experimental resolution [17,19]; the interest here is to present the complete available energy range.

The peak number 13_5 after $3d_{5/2}$ hole creation in Fig. 2(b), at 24.1 and 25.2 eV after $3d_{3/2}$ hole creation in Fig. 2(a) corresponds to a $4s^0 4p^6$ Kr^{2+} final state configuration as shown by Jauhiainen *et al.* [19]. Some additional peaks which are hidden in noncoincident experiments since they overlap with larger peaks coming from the other vacancy are directly separated in the coincident spectra. That is the case, for example, for the peak number 12_5, which is clearly seen in our coincidence spectrum in Fig. 2(b) but is almost hidden below peak number 13_3 in our noncoincident spectrum of Fig. 2(c). These filtered spectra extend other coincidence measurements by Hikosaka *et al.* [4] and Viefhaus *et al.* [6] and also confirm the identification of states previously proposed [16,18,19]. Even though our resolution is limited for energetic electrons, we can observe differences in the population of Kr^{2+} states, as a function of the $3d$ hole component: that is, the case for peaks 1 and 2 associated, respectively, with $4p^{-2}\ ^3P_2$ and $^3P_{1,0}$ states, where we confirm the previous observations [16] and calculations [17] indicating that peak 2 is more intense than peak 1 after $3d_{3/2}$ decay whereas it is the opposite after $3d_{5/2}$ decay. Our spectra include also the low-energy Auger transitions reported for the first time in the spectrum of Viefhaus *et al.* [6] taken at 101 eV photon energy. Our results are in good agreement. Above 12 eV, most of the peaks just appear to be shifted by spin-orbit splitting between the $3d_{3/2}$ and $3d_{5/2}$ spectra [Figs. 2(a) and 2(b)]. This is because they correspond to Auger decay from the $3d_{3/2}^{-1}$ and $3d_{5/2}^{-1}$ core-hole state to the same Kr^{2+} final states. It is no longer the case in low-energy range, where some peaks appear at the same energy positions independently of the initial inner-shell vacancy. This implies that these peaks come from the second step of a cascade

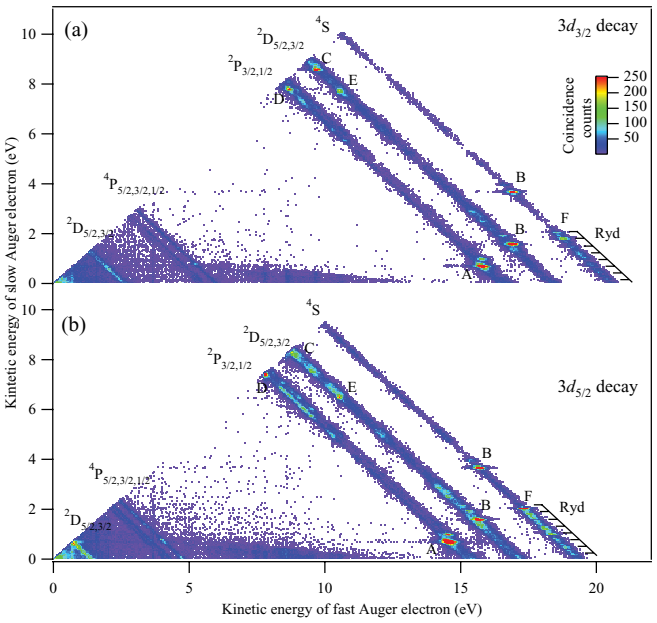

FIG. 3. (Color online) Two-dimensional picture, presenting the energy correlations between two Auger electrons detected in coincidence with a $3d_{3/2}$ photoelectron (a) or a $3d_{5/2}$ photoelectron (b). Counts (i.e., z axis in 2D picture) are given on a linear scale. The capital letters indicate the contribution of intermediate Kr^{2+} states, involved in cascade Auger decay. The states are labeled according to their intensity (i.e., A is the most intense; F is the weakest).

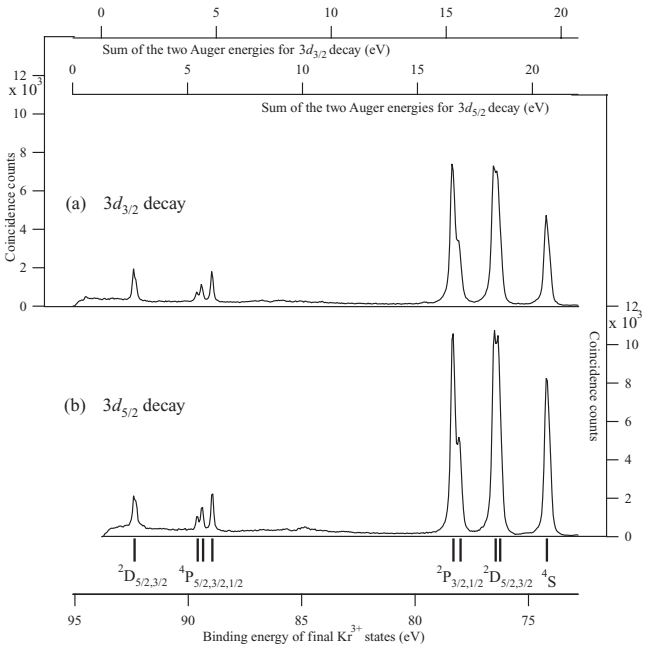

FIG. 4. Histograms of the sum of the two Auger energies emitted upon decay of a $3d$ hole, as deduced from integration along the diagonal lines of Fig. 3. The weak structure at a 85 eV binding energy comes from accidental coincidences visible in Fig. 3 involving a $3d$ photoelectron, an Auger electron, and a low-energy uncorrelated electron. Binding energies of the final Kr^{3+} states are deduced from those of the $3d$ levels by the Eq. (4). The calculated position of Kr^{3+} final states (vertical bars, bottom of the figure) are taken from NIST tables [32] after correction for the misprint in the value quoted for the Kr^{2+} ionization energy (289 020 cm^{-1} instead of 298 020 cm^{-1}); see text.

double-Auger decay, and correspond to the transition from one of the excited Kr^{2+*} states to a Kr^{3+} ion. This process will be discussed in more detail in the following section.

B. $3d$ decay by emission of two Auger electrons

Double-Auger decay of a Kr $3d$ hole has been much less studied than the single-Auger process. The first results were reported by Viefhaus *et al.* [6]. They measured coincidences between two of the three electrons emitted in the process (the $3d$ photoelectron and the two Auger electrons). The interest of our experiment is that all three emitted electrons are detected in coincidence, which eliminates all ambiguities that may remain. Our higher energy resolution, due to longer times of flight, and our high detection efficiency (down to zero energy electrons) bring significant improvement and allow the observation of minor decay channels.

Figure 3 shows 2D kinetic energy correlation maps between the two Auger electrons detected in coincidence with a $3d_{3/2}$ [Fig. 3(a)] or $3d_{5/2}$ [Fig. 3(b)] photoelectron. One observes mainly five diagonal lines in each spectrum with additional splitting due to the fine structure of the final Kr^{3+} state. Each diagonal line corresponds to a given Kr^{3+} final state and a constant amount of energy shared between the two Auger electrons. This excess energy represents the energy difference between the Kr^+ $3d^{-1}$ states and each final Kr^{3+} state:

$$\begin{aligned} E_{\text{Auger1}} + E_{\text{Auger2}} &= \text{const.} \\ &= (h\nu - E_{\text{3d Photoelectron}}) - E_{\text{B}}(\text{Kr}^{3+}) \\ &= E_{\text{B}}(\text{Kr}^{+}3d^{-1}) - E_{\text{B}}(\text{Kr}^{3+}), \end{aligned} \quad (4)$$

where E stands for kinetic energy and E_{B} for binding energy.

This also means that our experiment gives the absolute binding energies of the Kr^{3+} states populated by the double-Auger process with respect to the Kr^+ ($3d_{5/2}^{-1}$ or $3d_{3/2}^{-1}$) state as a reference. A less accurate method is to consider the energy balance between the three electrons and the photon. This latter method is less accurate since the energy resolution on the faster photoelectron (~30 eV) becomes the limiting factor compared to the resolution on the two slower Auger electrons. Figure 4 shows the summation of the 2D spectra of Fig. 3 along the $x = y$ diagonals, and displays the different Kr^{3+} final states observed in our experiment. The binding energy of the Kr^{3+} final states are deduced from the Eq. (4). The fine structure splitting of Kr^{3+} $4p^{-3}$ ^2P and ^2D states and Kr^{3+} $4p^{-2}4s^{-1}$ ^4P and ^2D is nearly resolved.

Our preliminary results [26] revealed that the value of the triple ionization threshold of krypton given in the literature at 75.308 eV [32,33,40] should be revised by more than 1 eV. Viefhaus *et al.* [6] positioned the Kr^{3+} threshold at 74.208 eV. Our present measurements locate the position of the triple ionization threshold Kr^{3+} ^4S ($4s^24p^3$) at 74.197 eV ± 20 meV in good agreement with the value given by Viefhaus *et al.* [6], and in reasonable agreement with the value of 74.03 ± 0.05 eV found by Eland *et al.* [34], which may be less accurate because deduced from the energy balance between the three electrons and the photon as discussed above. Our determination of the Kr^{3+} threshold relies on the position

of the Kr^+ $3d^{-1}$ states which are believed to be accurately known (within ±10 meV) from the measurements by King *et al.* [31]. Such a large error (>1.1 eV) for the Kr^{3+} threshold in the literature is rather surprising, considering the accuracy for other similar estimates. A closer examination traces the problem to the value adopted for the ionization potential of Kr^{2+} by Humphreys [40]; this value seems to be in reality overestimated by about 1.1 eV. The present NIST tables [32] use this value that Humphreys deduced from an extrapolation of the position of excited states of Kr^{2+} observed by optical spectroscopy in a plasma discharge [40]. This value has never been checked since that date and was also adopted by Sugar and Musgrove in their compilation of Kr energy levels [41]. The value given by Humphreys for the ionization potential of Kr^{2+} referenced to Kr^{2+} $4s^24p^4$ ($^3P_2$) ground state is 298 020 cm^{-1} (i.e., 36.95 eV). From our data we deduce a value for the Kr^{2+} ionization potential at 35.839 eV ± 20 meV (i.e., 289 061 cm^{-1}). This led us to propose that the origin of the discrepancy is a misprint in Humphreys' original paper: 289 020 cm^{-1} (instead of 298 020 cm^{-1}) would give 35.834 eV and a threshold for triple ionization at 74.192 eV in very close agreement with our determination. After this correction, our results concerning the energies of triply charged Kr are in very good agreement with the literature values, as shown in Fig. 4 where the Kr^{3+} binding energies given by NIST (after correction) are indicated.

The data from Fig. 4 also make it possible to deduce the probability that a 3*d* hole decays in a double-Auger process. Thanks to the nearly constant transmission of our spectrometer as a function of electron energies, it is deduced directly from the comparison of the total coincidence counts in Figs. 4 and 2. Taking into account the 54% ± 3% detection efficiency, we obtain for this double-Auger probability values of 28.4% ± 1% and 29.1% ± 1.1%, respectively, for the $3d_{5/2}$ and $3d_{3/2}$ decays, in good agreements with estimates from photoelectron-ion coincidence experiments [22,23].

Diagonal lines observed in the 2D spectra of Fig. 3 show some continuous background, but are clearly dominated by coincidence islands (spots). The continuous background is characteristic of a direct double-Auger process where two Auger electrons are emitted simultaneously and share the available energy continuously. The existence of spots (E_1, E_2) indicates that the two Auger electrons are emitted sequentially in a cascade double-Auger path proceeding by the creation of a short-lived Kr^{2+*} intermediate state. A close inspection of the various (E_1, E_2) spots in Fig. 3 allows us to reconstruct the different cascade paths, following the procedure described in [5]. In brief, the problem is to decide for each coincidence spot which electron, E_1 or E_2 is emitted first, by using the fact that a given intermediate Kr^{2+*} state is at the origin of several coincidence spots in Fig. 3. The result is that the majority of the cascade processes originate from six different Kr^{2+*} intermediate states that we label *A*, *B*, *C*, *D*, *E*, and *F* from the more intense to the weaker. One observes also a series of Kr^{2+*} states decaying to the Kr^{3+} (^4S) ground state, which we interpret as a Rydberg series converging onto the (^2D) Kr^{3+} state. Note that a similar Rydberg series was observed in the Xe 4*d* DA decay [5].

Figure 5 presents one-dimensional double-Auger spectra filtered according to both the initial 3*d* hole state and the Kr^{3+}

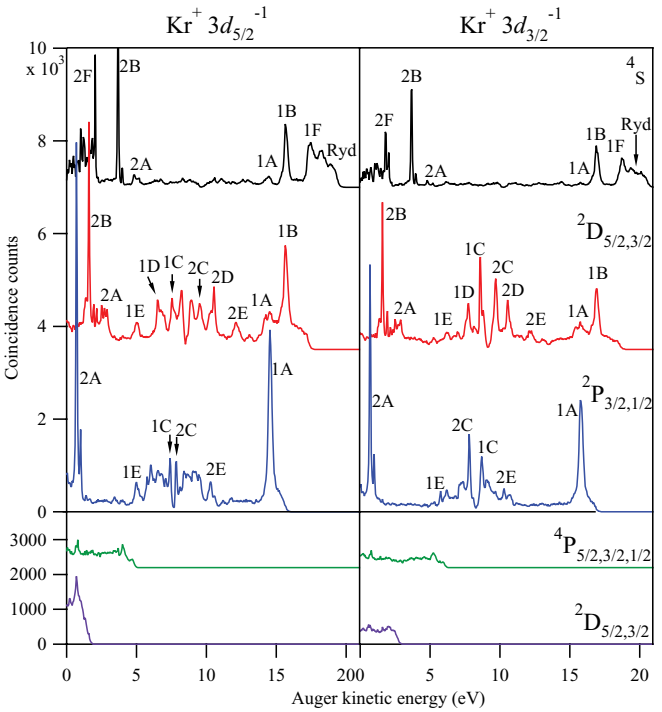

FIG. 5. (Color online) One-dimensional double-Auger spectra associated with the decay of a $3d_{5/2}$ (left) or a $3d_{3/2}$ (right) hole to a specific Kr^{3+} final state [from top to bottom, $(4p^{-3})^4S$, ^2D, ^2P, $(4s^{-1}4p^{-2})^4P$, and ^2D]. They are deduced from the projections of diagonal lines in Fig. 3 on the *x* and *y* axis. The minima in the middle of each spectrum at equal Auger energies result from the 20 ns dead time of the detector.

final states. The Kr^{3+} state is selected by fixing the energy sum $E = E_1 + E_2$ associated with the corresponding diagonal line of Fig. 3. The different coincidence spots of Fig. 3 appear now in Fig. 5 as peaks, and in each curve of Fig. 5 the first and second electrons emitted in a cascade transiting through the *X* Kr^{2+*} intermediate state are labeled as 1*X* and 2*X*. One notices in Fig. 5 that coincidences allow us to define exactly the starting point ($3d_{3/2}$ or $3d_{5/2}$ hole), the *X* Kr^{2+*} intermediate state, and the final point (^2P, ^2D or ^4S Kr^{3+*} state) of each cascade. The different one-dimensional double-Auger spectra of Fig. 5 appear to be symmetric around $E/2$. However, this symmetry is destroyed by two effects: first the experimental energy resolution ΔE depends on the kinetic energy ($\Delta E/E = 1.6\%$) and produces sharper slow-energy peaks; secondly, peak widths depend on the natural linewidths of both the 3*d* core-hole initial state and the intermediate *X* Kr^{2+*} state, and these linewidths have different effects on the peak shape associated to the first (1*X*) and the second (2*X*) electron of the cascade: 1*X* reflects both contributions whereas 2*X* is affected only by the linewidth of the *X* Kr^{2+*} intermediate state.

One sees that from our data it is possible to reconstruct the cascade paths involved in the double-Auger decays. The information we could extract is given in Table II and schematically presented in Fig. 6. It includes branching ratios for population of each intermediate Kr^{2+} state from the initial $3d_{3/2}$ or $3d_{5/2}$ hole and branching ratios for the decay of each Kr^{2+} intermediate state to the final Kr^{3+} states. Note that in a

TABLE II. Properties of Kr^{2+} states involved in double-Auger decays of 3*d* holes. The binding energy of the Kr^{2+} states is deduced from the measurement at high-energy resolution of the last electron emitted in the cascade Auger decay (from Figs. 7 and 8). The final state reached in the cascade decay is identified thanks to the coincidence measurements by comparing spectra of Fig. 5 to Fig. 7, and is indicated in the third column of the table. As explained in the text, the absolute binding energies of the Kr^{2+} states are expected to be accurate within ±20 meV, but their relative energies are expected to be more accurate, within ±2 meV.

Kr^{2+} state	Binding energy (eV)	2nd-step Auger used from Fig. 7 in Kr^{2+} determination Kinetic energy | Kr^{3+} final state		Lifetime broadening (meV)	Branching ratio for decay to Kr^{3+} states		
					^4S	^2D (%)	^2P
Ryd					100	0	0
F	76.269	2.072	^4S		100	0	0
	77.909	1.600	$^2D_{3/2}$	3.6 ± 1			
		3.710	^4S		30	70	0
B	77.939	1.631		6.6 ± 1			
	77.975	1.667		7.6 ± 1			
A	79.066	0.727	$^2P_{3/2}$	73 ± 4	4	17	79
C	85.218	8.703	$^2D_{5/2}$				
D	86.249	7.911	$^2P_{1/2}$		0	49	51
E	87.205	10.690	$^2D_{5/2}$				

two-step description these last branching ratios should be the same whether the intermediate Kr^{2+} state has been populated by decay of the $3d_{3/2}$ or $3d_{5/2}$ hole, and we used both values for the final estimates in Table II. It is also possible to obtain from our measurements the binding energy of the intermediate *X* Kr^{2+} states. We used for these estimates the measured values of the 2*X* peak corresponding to the second electron emitted in the cascade. The binding energy of the *X* Kr^{2+} state is then obtained by adding the 2*X* value to the binding energies of the corresponding Kr^{3+} final state ($^2P_{3/2}$, $^2P_{1/2}$, $^2D_{5/2}$, $^2D_{3/2}$, or ^4S).

In order to obtain the 2*X* peaks with a better resolution, we used a high-performance hemispherical electron energy analyzer MBS-A1 to measure the noncoincident 3*d* Auger

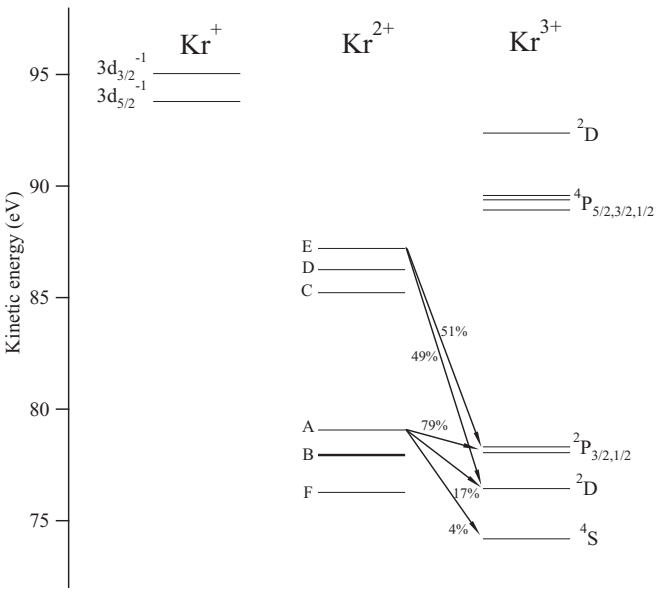

FIG. 6. Schematic representation of the main cascade paths involved in the 3*d* double-Auger decays. Branching ratios are given for the most important decays. The Kr^{2+} *A* state, for example, evolves mainly to $Kr^{3+2}D$ and ^2P states.

electron spectrum in the energy range associated with double-Auger decay. The result shown in Fig. 7 (top curve) combines measurements performed at 101 and 105 eV photon energies with an experimental energy resolution of 14 meV. It is compared with the "reconstructed" coincident Auger spectra, obtained after summation of all spectra displayed in Fig. 5 for each initial hole: $3d_{3/2}$ middle curve (blue), $3d_{5/2}$ bottom curve (red). The improvement in resolution for all 2*X* peaks is clear and allows us to propose in Table II precise values for the binding energy of Kr^{2+} states involved in cascade decays. Note that the relative positions should be correct within ±2 meV (a fraction of the total experiment resolution) whereas absolute positions reflect the ±20 meV uncertainty linked to our procedure to locate the Kr^{3+} (^4S) ground state. The high resolution enables one to observe also the fine structure in the Kr^{2+} states, such as the three components observed for the "*B*" Kr^{2+} state that could possibly reflect the spin-orbit structure. Finally, it was possible to measure with an increased resolution a part of the noncoincident Auger spectrum. Results are given in Fig. 8 which zooms in on the 0–2.5 eV energy range with an expected 3.2 meV experimental resolution, linked to the 5 eV pass energy we used. It is then possible in favorable cases to observe the lifetime broadening and estimate the lifetime of the Kr^{2+} intermediate states. One deduces a lifetime of 9 ± 0.4 fs (73 ± 4 meV natural broadening) for the *A* state and of 190 ± 40, 100 ± 10, and 87 ± 7 fs (3.6 ± 0.7, 6.6 ± 0.6, and 7.6 ± 0.7 meV lifetime broadening) for the three components of the *B* state. Note that these different lifetimes may result from the different coupling in the spin-orbit component of the Kr^{2+} *B* electronic state, and do not necessarily imply that we have contribution of different possibly unresolved electronic states. These lifetimes have to be compared to the lifetime of the 3*d* hole states, which amount to 7.5 ± 0.4 fs (88 ± 4 meV natural broadening) [24].

V. COMPARISON WITH THEORY

After the production of 3*d* vacancy only doubly and triply charged ions of krypton are obtained [23]. In fact, the

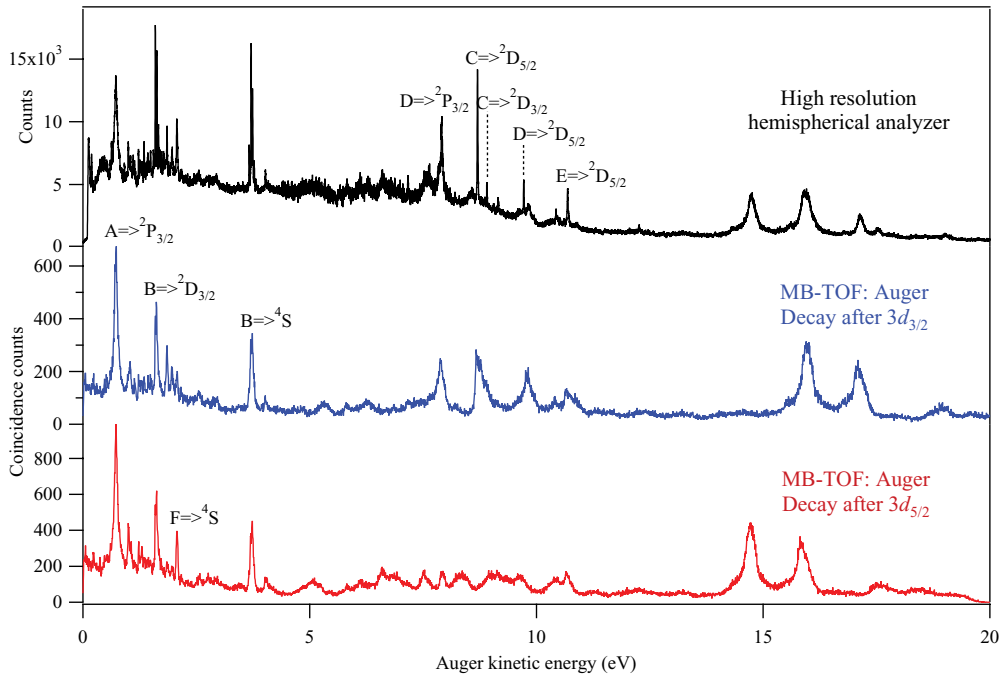

FIG. 7. (Color online) (Top) Noncoincident Kr 3*d* Auger spectrum in the 0–20 eV energy range associated with double-Auger decays. It was obtained at UVSOR with a high-resolution MBS-A1 hemispherical analyzer with a 14 meV resolution. It is compared with coincident spectra deduced from Fig. 5. Assignment of the main second-step Auger lines is reported with a $X = >L_J$ notation where X refers to the intermediate Kr^{2+} states given in Table II, and L_J refers to the term of the Kr^{3+} $4p^{-3}$ final state.

quadruple ionization threshold can be estimated at 126.7 eV (from our value of Kr^{3+} threshold and the NIST value given for the Kr^{3+} ionization potential [32]) and could only be reached after $3d^{-1}4s^{-1}$ core-valence double ionization. The result of our calculations for the main branches of all Auger cascades following initial $3d^{-1}$ states are shown in Fig. 9 ($3d_{3/2}$ on the upper part, $3d_{5/2}$ on the lower part of the figure) and reported in Table I. A level is assigned to a given configuration according to the largest weight in the expansion of the wave function. The $j = 3/2$ and $j = 5/2$ cascades are very similar. The branching ratios for most transitions differ by less than 10%; the largest difference is obtained for $3d^9 \rightarrow 4s4p^5 + e^-$ transitions. Due to the strong mixing of configurations, especially between $4s4p^5$ and $4s^24p^34d$, many-electron Auger transitions become important. The discrete double transitions (with one electron ejected and another excited) $3d^9 \rightarrow 4s^24p^34d + e^-$ play an

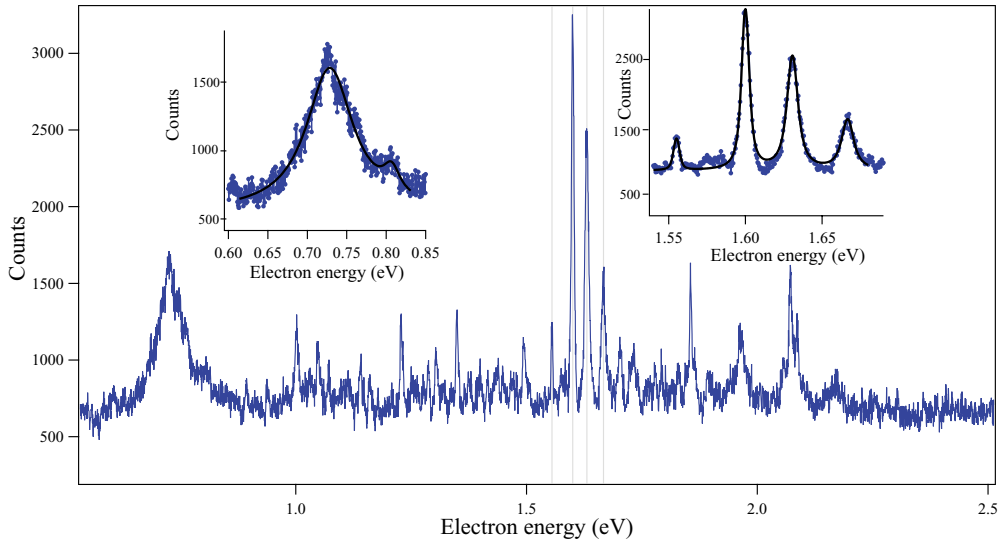

FIG. 8. (Color online) High-resolution 3*d* Auger spectrum obtained with the MBS-A1 hemispherical analyzer at a pass energy of 5 eV giving an expected experimental resolution of 3.2 meV. The inserts present the fit by a Voigt profile of the peak at 0.727 eV with a Lorentzian width of 73 meV ($T = 9$ fs) and of series of peaks at (1.600, 1.631, and 1.667 eV) with Lorentzian widths estimated at (3.6 ± 1, 6.6 ± 1, and 7.7 ± 1 meV), respectively, corresponding, respectively, to lifetimes 150–230, 90–110, and 80–95 fs.

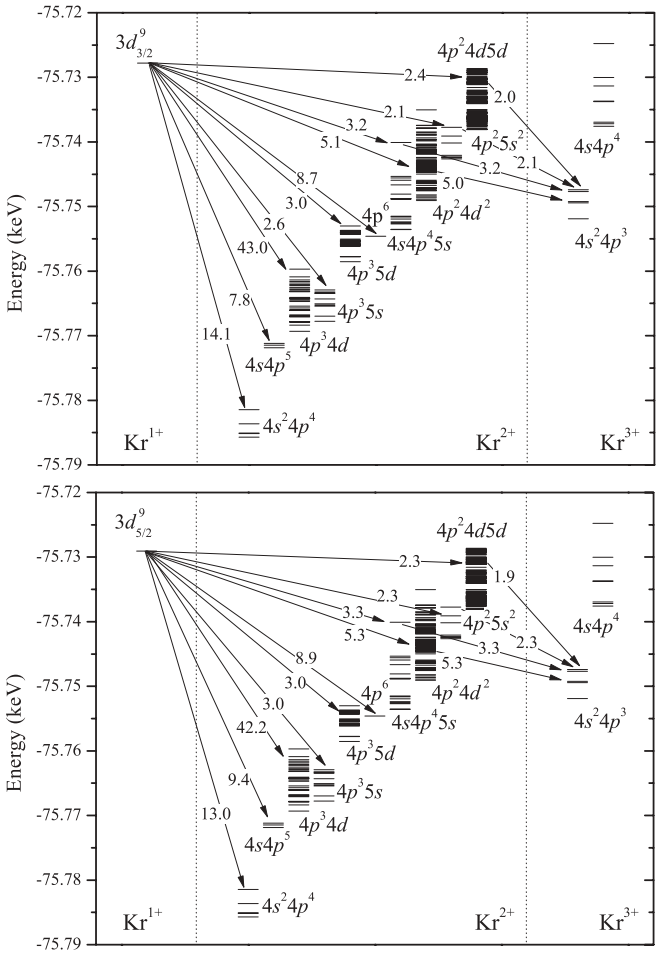

FIG. 9. Theoretical calculations of the Auger decays following the $3d_{3/2}^{-1}$ (top) and $3d_{5/2}^{-1}$ (bottom) state decay in Kr. The numbers on the arrows indicate the branching ratios in %. Only the main branches with ratios exceeding 1% are indicated.

essential role in the production of Kr^{2+} ions. The most accurate information on many-electron Auger transitions during this cascade was given in Jonauskas *et al.* [21]; the detailed level-by-level calculation in CI approximation enabled us to reduce the discrepancies between previous theoretical results [42] and experiment (Refs. [22,23] and present measurements) for the relative yields of Kr^{3+} ions: the calculated relative yield increased from 1.2% to 20% while the experimental value is about 30%. The comparison of the part of these cascades corresponding to the double-Auger transitions with the scheme presented in Fig. 9 indicates the possible configurations of the intermediate states for the most important decays denoted by the capital letters (*A*, *B*, *C*, *D*, *E*) in Fig. 6. These configurations are also reported in Table I. However, due to some energy shifts between calculated and experimental values, the accurate identification of the intermediate states can be obtained only from the investigation of Auger transition intensities. The description of the most populated intermediate Kr^{2+*} states involved in cascade Auger processes involves also an important contribution of the $4s^{-2}$ configuration, even if this configuration is not the dominant one in the wave-function expansion. The calculations of Aksela *et al.* [18] already indicated that several satellite states correlate with this $4s^{-2}$ configuration. Our calculations show that intense peak 27 (Fig. 10) from the second stage of Auger cascade is a result of mixing of $4s^{-2}$ and $4s^{-1}4p^{-2}5s$ configurations. Note that in the case of the formation of $4s^{-2}$ satellite states the double-Auger process begins with a single-Auger process involving only the interaction between the two 4*s* electrons: after 3*d* inner-shell ionization, one 4*s* electron fills the inner-shell hole, whereas the second 4*s* electron is emitted. The doubly charged excited state of krypton with strong $4s^{-2}$ configuration afterwards decays by autoionization. Similar processes have been observed in xenon 4*d* [5] and argon 2*p* [10] cases that involve also electrons from inner valence shells. To summarize, cascade Auger decay is the predominant process, compared to direct double-Auger decay where the electrons share the available energy. Cascade Auger decay after a given *nl* inner-shell ionization comes from intermediate states populated by a two-electron process involving two $(n+1)s$ electrons: for krypton 3*d* hole, mainly the 4*s* electrons participated; for argon 2*p* hole, two 3*s* electrons were involved; whereas for xenon 4*d* inner-shell ionization, 5*s* electrons had a major contribution in the double-Auger cascades. The first Auger decay in the cascade implies only two electron correlations and this process is not negligible.

Figure 10(b) presents the calculated total spectra of Auger transitions including first (in black) and second (in red) stages in the cascade from the $3d_{3/2}^{-1}$ and $3d_{5/2}^{-1}$ initial states. They reproduce the experimental spectra recorded in coincidence with the $3d_{3/2}$ and $3d_{5/2}$ photoelectrons fairly well [as presented in Fig. 2 and redrawn in Fig. 10(a)]. Comparison with the result of previous calculations shown in Fig. 10(c) shows a great improvement in the reliability of theoretical calculations. The peaks of transitions from the initial $3d_j^{-1}$ states cover the whole range of the spectrum. At energies below ~20 eV some small contributions from the second-stage transitions already appear. The structure of the spectrum in the interval 5–13 eV results from the first and second step strongly overlapping Auger transitions. Only below 5 eV is the spectrum predicted to be dominated by the lines of the second stage. All peaks of the calculated spectrum are shifted to higher energy with respect to the experimental peaks (this corresponds to the known effect of the widening of the spectrum calculated by the *ab initio* method due to noninclusion of the interaction with many highly excited configurations). This shift varies from 0.5 to 2.5 eV for transitions between various configurations; the larger values correspond to transitions of the second stage. The most intense Auger lines of the 3*d* Auger spectrum were identified by Werme *et al.* [16] and Jauhiainen *et al.* [19] from the interpretation of noncoincident spectra. The present comparison of the results of large-scale calculation with the experimental coincidence spectra gives the opportunity to identify practically all structure in the spectrum, including its part below 22 eV recorded in this work. The $3d_{3/2}$ and $3d_{5/2}$ spectra have similar structure, thus the same numbers identifying the same Kr^{2+} final state are attributed to the corresponding peaks in both spectra of Figs. 2 and 10 with indexes 5 and 3 for $3d_{5/2}$ or $3d_{3/2}$. Most of the peaks, especially in the low-energy range, originate from several transitions and their states usually correspond to the superposition of various terms. Their mixing is rather strong in the *jj* coupling scheme used in our relativistic calculations. Thus, in Table I we

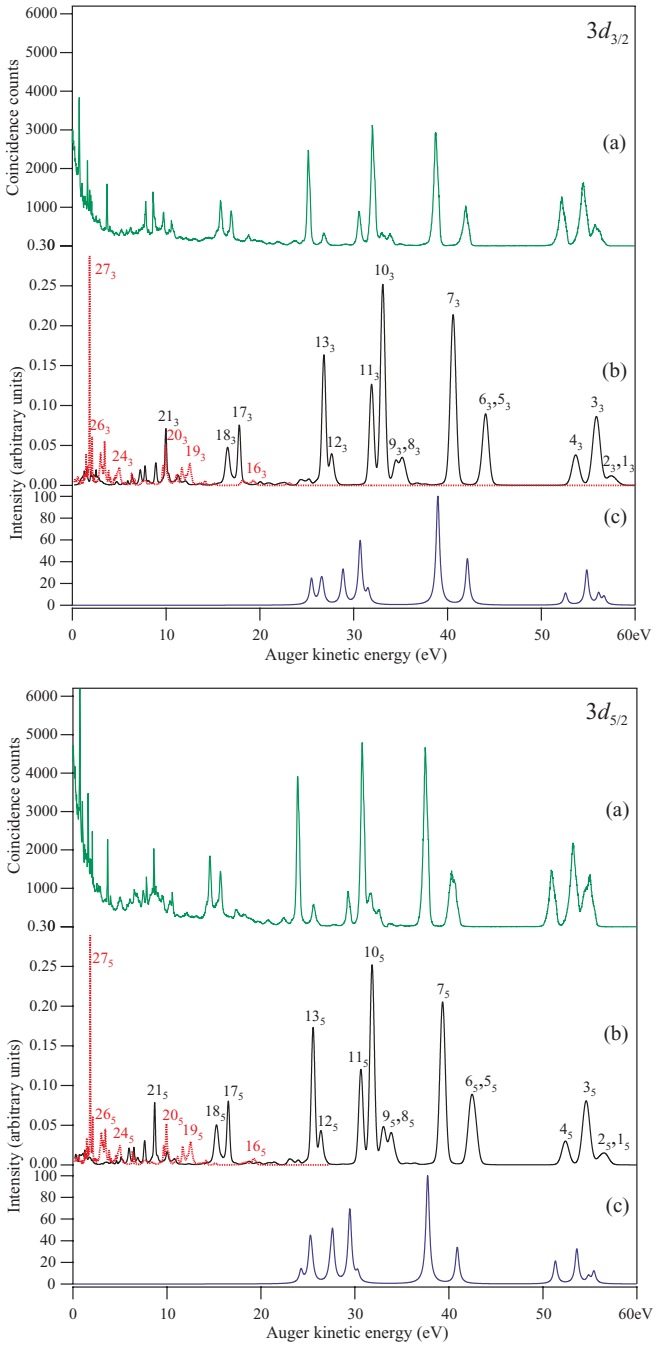

FIG. 10. (Color online) Summary of Auger spectra. Present experimental work (upper part, in green) is redrawn from Fig. 2(a). The theoretical Auger spectra of the first (black line) and second (red dashed line) stages of cascades are given in the middle part of the figures (b). The upper graph corresponds to the $3d_{3/2}^{-1}$ state decay, whereas the lower part corresponds to the $3d_{5/2}^{-1}$ state decay. Previous calculated spectra of the literature [17–19] are given (in blue) in the lower part (c). Note that for curve (c) the peak widths corresponds to the $3d$ lifetime only and do not include the experimental resolution which is included in (a) and (b).

indicate only the configurations giving the main contribution to the corresponding peak. The designation of some symbols introduced in Figs. 3 and 5 of this work are indicated in this table, too.

Among the more intense peaks associated with cascade DA decay identified in this work we notice peak number 17 corresponding to the transitions $3d^{-1} \rightarrow 4s4p^4 5s + e^-$ (B state) and peak number 18, corresponding to $3d^{-1} \rightarrow 4p^2 4d^2 + e^-$ transitions (A state).

Almost all of the most intense peaks of the second step of an Auger cascade correspond to $4p^2 4d^2 \rightarrow 4p^3 + e$ transitions; the only exceptions are peak numbers 20 and 27, originating from $4p^2 5\,s^2 \rightarrow 4p^3 + e$ and $4s4p^4 5s \rightarrow 4p^3$ transitions, respectively. The $4p^2 4d^2$ configuration contains many close-lying levels and only transitions from some of them to the levels of the $4p^3$ configuration are energetically allowed. For this reason, the results of calculation of the second spectrum are rather sensitive to the correlation effects. It is necessary to note also the same feature for peak number 11, whose intensity strongly depends on the configuration basis used for the initial $3d_j^{-1}$ state.

The calculation reveals that most peaks in the low-energy part of the spectra are due to transitions from first and second stages. For peak number 16, transitions of the two kinds are indicated. The wide peak number 16 is formed by many Auger transitions to the Rydberg states: $3d^9 \rightarrow 4p^3\ nd$ ($n = 8$–11) and from the Rydberg states $4s^1 4p^4\ nd$ ($n = 5$–11) to the levels of the $4p^3$ configuration (easily identified in the second step decay to ^4S in Figs. 3 and 5). The additional structure of the calculated peak numbers 14 and 23 is probably caused by the energy shift $E_{\text{calc}} - E_{\text{exp}}$, mentioned above, that differs for various lines.

According to Figs. 4 and 9 the triply charged krypton ions are mainly obtained through the cascade Auger decay ending in the $4p^3$ configuration of Kr^{3+}. The results of our calculations for the population of the Kr^{3+} final states produced in cascade DA decays is reported in Fig. 11 (bars) and compared to the experimental results from Fig. 4. The distribution of Kr^{3+} ions in various terms of $4p^3$ configuration

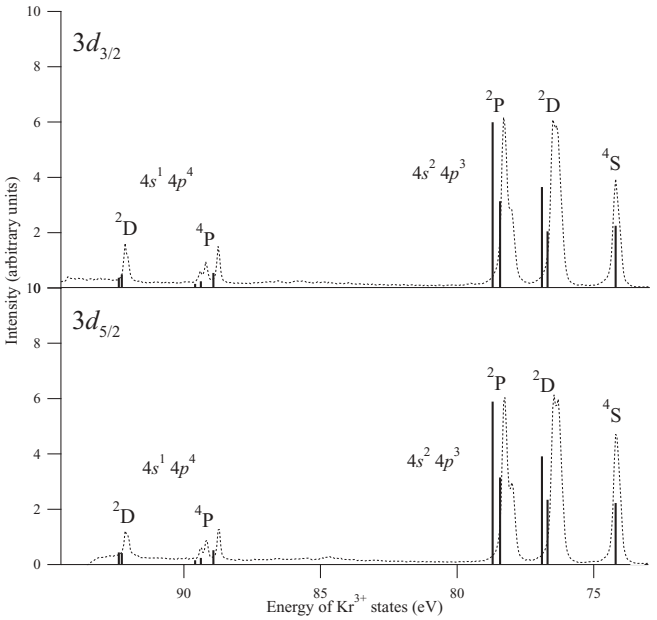

FIG. 11. Population of the Kr^{3+} final states produced in DA decays. Solid lines give the calculated intensities while dashed lines give the experimental spectrum from Fig. 4.

corresponds approximately with the experimental data, but the populations of ^2D and ^4S appear underestimated with respect to ^2P. Energetically, some levels of Kr^{2+} can also decay to Kr^{3+} states of the $4s^14p^4$ configuration; their calculated relative total population is about 1.8%. This is lower than the experimental values of 6.2% and 7.7%, respectively, for the $3d_{5/2}$ and $3d_{3/2}$ decays, and suggests that a direct double-Auger process, not included in our calculations, could be important for the formation of these excited $4s^14p^4$ Kr^{3+} states. This is also in agreement with the relative flat energy distributions of the associated one-dimensional double-Auger spectra of Fig. 5.

VI. CONCLUSION

Multicoincidence spectroscopy has allowed us to disentangle the Auger decays following $3d$ inner-shell ionization of krypton. Single-Auger decays can be separately attributed to the initial $3d_{5/2}$ or $3d_{3/2}$ core-hole state. The study of double-Auger decays shows that the Kr^{3+} threshold is more than 1.1 eV lower than in the literature, an error which probably results from a misprint in the original paper. We find the Kr^{3+} ^4S ionization threshold at 74.197 ± 0.020 eV, in good agreement with recent estimates [6,34]. The main Kr^{2+*} states involved in double-Auger decays consecutive to a Kr $3d$ hole have been observed and assigned. The mechanism of the cascade double-Auger decay involves $4s^{-2}$ correlations satellites that are populated efficiently in a first Auger process and decay later by autoionization since they lie above the Kr^{3+} thresholds. The comparison of our large-scale calculations with the experimental coincidence $3d_j$ Auger spectra enables us to identify almost all their structure, including the part of the spectrum below 22 eV recorded at very high resolution. The structure of spectra in the interval 5–13 eV is formed by strongly overlapping Auger lines of both stages, while only below 5 eV do lines of the second stage dominate. The discrete Auger transitions play a more important role in the formation of triple krypton ions than direct double-Auger transitions; their contribution to the spectra is more significant at small energies, especially for the transitions to the $4s4p^4$ configuration. In the course of preparation of this paper we learnt that a complementary paper was submitted to Physical Review A [43].

ACKNOWLEDGMENTS

This work was supported by the European Community–Research Infrastructure Action under the FP6 "Structuring the European Research Area" Programme through the Integrated Infrastructure Initiative "Integrating Activity on Synchroton and Free Electron Laser Science," Contract No. R II 3-CT-2004-506008. This work was also supported in part by Lithuanian Research Council, Contract No. MIP-10107. P. Lablanquie thanks the hospitality of UVSOR staff during part of this work. We warmly acknowledge the support by the beam line scientists (B. Zada and W. Mahler) and our colleagues J. Viefhaus and M. Braune who made possible these experiments at BESSY.

[1] T. A. Carlson and M. O. Krause, Phys. Rev. Lett. **14**, 390 (1965).
[2] R. Püttner, V. Sekushin, G. Kaindl, X.-J. Liu, H. Fukuzawa, K. Ueda, T. Tanaka, M. Hoshino, and H. Tanaka, J. Phys. B: At. Mol. Opt. Phys. **41**, 045103 (2008).
[3] P. Lablanquie, F. Penent, R. I. Hall, H. Kjeldsen, J. H. D. Eland, A. Muehleisen, P. Pelicon, Z. Smit, M. Zitnik, and F. Koike, Phys. Rev. Lett. **84**, 47 (2000).
[4] Y. Hikosaka, F. Penent, P. Lablanquie, R. I. Hall, and K. Ito, Meas. Sci. Technol. **11**, 1697 (2000).
[5] F. Penent, J. Palaudoux, P. Lablanquie, L. Andric, R. Feifel, and J. H. D. Eland, Phys. Rev. Lett. **95**, 083002 (2005).
[6] J. Viefhaus, M. Braune, S. Korica, A. Reinköster, D. Rolles, and U. Becker, J. Phys. B: At. Mol. Opt. Phys. **38**, 3885 (2005).
[7] P. Bolognesi, M. Coreno, A. De Fanis, V. Feyer, S. Turchini, N. Zema, T. Prosperi, and L. Avaldi, AIP Conf. Proc. **811**, 138 (2006).
[8] S. Sheinerman, P. Lablanquie, F. Penent, J. Palaudoux, J. H. D. Eland, T. Aoto, Y. Hikosaka, and K. Ito, J. Phys. B: At. Mol. Opt. Phys. **39**, 1017 (2006).
[9] Y. Hikosaka, T. Aoto, P. Lablanquie, F. Penent, E. Shigemasa, and K. Ito, J. Phys. B: At. Mol. Opt. Phys. **39**, 3457 (2006).
[10] P. Lablanquie, L. Andric, J. Palaudoux, U. Becker, M. Braune, J. Viefhaus, J. H. D. Eland, and F. Penent, J. Electron Spectrosc. Relat. Phenom. **156-158**, 51 (2007).
[11] Y. Hikosaka, P. Lablanquie, F. Penent, T. Kaneyasu, E. Shigemasa, J. H. D. Eland, T. Aoto, and K. Ito, Phys. Rev. A **76**, 032708 (2007).
[12] J. Palaudoux, P. Lablanquie, L. Andric, J. H. D. Eland, and F. Penent, J. Phys.: Conf. Ser. **141**, 012012 (2008).
[13] V. Ulrich, S. Barth, S. Joshi, T. Lischke, A. M. Bradshaw, and U. Hergenhahn, Phys. Rev. Lett. **100**, 143003 (2008).
[14] J. H. D. Eland, Adv. Chem. Phys. **141**, 103 (2009).
[15] W. Mehlhorn, Z. Phys. **187**, 21 (1965).
[16] L. O. Werme, T. Bergmark, and K. Siegbahn, Phys. Scr. **6**, 141 (1972).
[17] E. J. Mc Guire, Phys. Rev. A **11**, 17 (1975).
[18] H. Aksela, S. Aksela, and H. Pulkkinen, Phys. Rev. A **30**, 2456 (1984).
[19] J. Jauhiainen, H. Aksela, S. Aksela, A. Kivimaki, O. P. Sairanen, E. Nommiste, and J. Vegh, J. Phys. B: At. Mol. Opt. Phys. **28**, 3831 (1995).
[20] L. Partanen, M. Huttula, H. Aksela, and S. Aksela, J. Phys. B: At. Mol. Opt. Phys. **40**, 3795 (2007).
[21] V. Jonauskas, R. Karazija, and S. Kučas, J. Phys. B: At. Mol. Opt. Phys. **41**, 215005 (2008).
[22] S. Brünken, C. Gerth, B. Kanngiesser, T. Luhmann, M. Richter, and P. Zimmermann, Phys. Rev. A **65**, 042708 (2002).
[23] Y. Tamenori, K. Okada, S. Tanimoto, T. Ibuki, S. Nagaoka, A. Fujii, Y. Haga, and I. H. Suzuki, J. Phys. B: At. Mol. Opt. Phys. **37**, 117 (2004).
[24] M. Jurvansuu, A. Kivimäki, and S. Aksela, Phys. Rev. A **64**, 012502 (2001).

[25] F. Penent, S. Sheinerman, L. Andric, P. Lablanquie, J. Palaudoux, U. Becker, M. Braune, J. Viefhaus, and J. H. D. Eland, J. Phys. B **41**, 045002 (2008).
[26] P. Lablanquie, F. Penent, J. Palaudoux, L. Andric, T. Aoto, K. Ito, Y. Hikosaka, R. Pfeifel, and J. H. D. Eland, in Proceedings XXIV ICPEAC, Rosario, Argentina, 148, 2005.
[27] J. Palaudoux, Ph.D. thesis, Université Pierre et Marie Curie, 2006.
[28] J. H. D. Eland, O. Vieuxmaire, T. Kinugawa, P. Lablanquie, R. I. Hall, and F. Penent, Phys. Rev. Lett. **90**, 053003 (2003).
[29] Y. Hikosaka, P. Lablanquie, F. Penent, T. Kaneyasu, E. Shigemasa, R. Feifel, J. H. D. Eland, and K. Ito, Phys. Rev. Lett. **102**, 013002 (2009).
[30] K. Ito, F. Penent, Y. Hikosaka, E. Shigemasa, I. H. Suzuki, J. H. D. Eland, and P. Lablanquie, Rev. Sci. Instrum. **80**, 123101 (2009).
[31] G. C. King, M. Tronc, F. H. Read, and R. C. Bradford, J. Phys. B: At. Mol. Opt. Phys. **10**, 2479 (1977).
[32] Y. Ralchenko, A. E. Kramida, and J. Reader (NIST ASD team), *NIST Atomic Spectra Database*, version 3.1.5 [http://physics.nist.gov/asd3] [June 16, 2010]. (National Institute of Standards and Technology, Gaithersburg, 2008).
[33] E. B. Saloman, J. Phys. Chem. Ref. Data **36**, 215 (2007).
[34] J. H. D. Eland, P. Linusson, L. Hedin, E. Andersson, J.-E. Rubensson, and R. Feifel, Phys. Rev. A **78**, 063423 (2008).
[35] G. Gamblin, Ph.D. thesis, Université Pierre et Marie Curie, 2009.
[36] M. F. Gu, Astrophys. J. **582**, 1241 (2003).
[37] R. Karazija, *Sums of Atomic Quantities and Mean Characteristics of Spectra (*Mokslas, Vilnius, 1991) [in Russian].
[38] S. Kučas, V. Jonauskas, and R. Karazija, Phys. Scr. **55**, 667 (1997).
[39] M. R. Zaghloul, Mon. Not. R. Astron. Soc. **375**, 1043 (2007).
[40] C. J. Humphreys, Phys. Rev. **47**, 712 (1935).
[41] J. Sugar and A. Musgrove, J. Phys. Chem. Ref. Data **20**, 859 (1991).
[42] A. G. Kochur, A. I. Dudenko, and D. J. Petrini, J. Phys. B **35**, 395 (2002).
[43] E. Andersson *et al.*, Phys. Rev. A **82**, 043418 (2010).